

Magnetic structure of Tb_3RuO_7 possessing alternating-bond spin- $\frac{3}{2}$ Ru chains in a nonuniform internal magnetic field: appearance of a partially disordered state

Masashi Hase^{1,*}, Andreas Dönni², and Vladimir Yu. Pomjakushin³

¹*Research Center for Advanced Measurement and Characterization,*

National Institute for Materials Science (NIMS),

1-2-1 Sengen, Tsukuba, Ibaraki 305-0047, Japan

²*International Center for Materials Nanoarchitectonics (WPI-MANA),*

National Institute for Materials Science (NIMS),

1-1 Namiki, Tsukuba, Ibaraki 305-0044, Japan

³*Laboratory for Neutron Scattering and Imaging,*

Paul Scherrer Institut (PSI), CH-5232 Villigen PSI, Switzerland

(Dated: September 30, 2021)

Abstract

We report on the magnetic structures of Tb_3RuO_7 and Nd_3RuO_7 determined from powder neutron-diffraction experiments. In Tb_3RuO_7 , alternating-bond spin- $\frac{3}{2}$ Ru1-Ru2 chains are formed. The Ru1 and Ru2 moments are ordered and disordered (paramagnetic), respectively, below 15 K. This result indicates the appearance of a partially disordered (PD) state, although the two Ru sites are very similar to each other. In Nd_3RuO_7 , the Ru1 and Ru2 ions form independent uniform chains. Both the Ru1 and Ru2 moments are ordered below 17.5 K. Probably, the main source of the PD state in Tb_3RuO_7 is the magnetic frustration in the exchange interactions. The internal magnetic field generated by the Tb ordered moments at the Ru1 sites is different from that at the Ru2 sites. We speculate that the different (nonuniform) internal magnetic field enhances the difference in the properties between the Ru1 and Ru2 moments. We also report on the magnetic entropy changes of Tb_3RuO_7 and Gd_3RuO_7 .

PACS numbers: 75.25.-j, 75.10.Pq, 75.47.Lx, 75.30.Sg

*Electronic address: HASE.Masashi@nims.go.jp

I. INTRODUCTION

Spin chains to which a nonuniform magnetic field is applied are expected to exhibit exotic properties. For example, a staggered magnetic field is induced by a uniform external magnetic field at the spin chain with an alternating g tensor and the antisymmetric interaction of the Dzyaloshinsky–Moriya (DM) type with an alternating D vector. The staggered magnetic field is known to appear in real materials such as $\text{Cu}(\text{C}_6\text{H}_5\text{COO})_2 \cdot 3\text{H}_2\text{O}$ (copper benzoate) [1–4], $\text{CuCl}_2 \cdot 2[(\text{CD}_3)_2]$ [5, 6], Yb_4As_3 [7, 8], $\text{PM} \cdot \text{Cu}(\text{NO}_3)_2 \cdot (\text{H}_2\text{O})_2$ (PM = pyrimidine) [9–12], and KCuGaF_6 [13–16]. Low-energy properties can be represented by the quantum sine-Gordon model. Excitations of the solitons and breathers were observed in KCuGaF_6 [16].

A nonuniform magnetic field can also be applied to the following spin chains: different crystallographic magnetic-ion sites in the spin chains and other magnetic-ion sites outside the spin chains. When magnetic moments on the magnetic-ion sites outside the spin chains are ordered, a different (nonuniform) internal magnetic field is applied to the magnetic-ion sites in the spin chains.

We focus on Tb_3RuO_7 , Gd_3RuO_7 , and Nd_3RuO_7 possessing spin- $\frac{3}{2}$ chains formed by the Ru^{5+} ($4d^3$) ions. The three compounds are isostructural in the high-temperature (T) phase. The space group is $Cmcm$ (No. 63) [17–21]. In Tb_3RuO_7 , Gd_3RuO_7 , and Nd_3RuO_7 , a structural phase transition occurs at $T_s = 402$, 380, and 130 K, respectively, [22] and the space groups of the low- T phase are $Pna2_1$ (No. 33) [17], $Pna2_1$ (No. 33) [23], and $P2_1/m$ (No. 11) [21], respectively. In the low- T phase, Tb_3RuO_7 and Gd_3RuO_7 are isostructural.

We describe the arrangements of the Ru sites and changes in the Ru and rare-earth (R) sites owing to the structural phase transition. In the high- T phase, the Ru site is unique and uniform Ru chains are formed. In each low- T phase, two crystallographic Ru (Ru1 and Ru2) sites exist. However, the two Ru sites are very similar to each other. Figure 1 shows the crystal structure of the low- T phase of Tb_3RuO_7 . An alternating-bond chain parallel to the b direction is formed by the Ru1 and Ru2 ions. In the two types of Ru1-Ru2 pairs, the Ru1-Ru2 length and Ru1-O-Ru2 angle at room temperature are 3.67 Å and 141.6°, and 3.68 Å and 145.5°. From the angles, antiferromagnetic (AF) exchange interactions are expected in the Ru1-Ru2 pairs. When the Tb magnetic moments are ordered, different (nonuniform) internal magnetic fields are applied to the Ru1 and Ru2 sites. In Nd_3RuO_7 , the Ru1 and

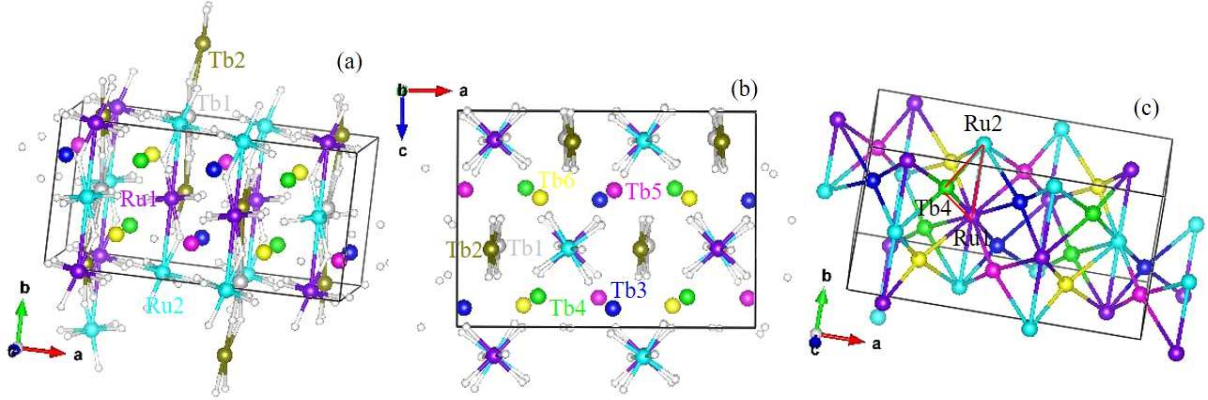


FIG. 1: (a)(b) Crystal structure of the low- T phase of Tb_3RuO_7 , drawn using VESTA [24]. The orthorhombic space group is $Pna2_1$ (No. 33) [17]. The lattice constants are $a = 14.588 \text{ \AA}$, $b = 7.345 \text{ \AA}$, and $c = 10.560 \text{ \AA}$ at room temperature. The rectangle represents a unit cell. All the ions are located at the $4a$ sites. There are two crystallographic Ru sites and six crystallographic Tb sites. The y coordinates are nearly 0 and 0.5 at the Ru1, Ru2, Tb1, and Tb2 sites. They are nearly 0.25 and 0.75 at the Tb_i ($i = 3 - 6$) sites. Alternating-bond chains parallel to the b direction are formed by the Ru1 and Ru2 ions and by the Tb1 and Tb2 ions. The crystal structure of the low- T phase of Nd_3RuO_7 is similar to that of Tb_3RuO_7 . The following is a remarkable difference between the two compounds. In Nd_3RuO_7 with the monoclinic space group $P2_1/m$ (No. 11), the Ru1 and Ru2 ions form independently uniform chains parallel to the b direction. Similarly, the Nd1 and Nd2 ions form independently uniform chains parallel to the b direction. (c) Schematic of Ru1, Ru2, and Tb_i ($i = 3 - 6$) sites. Magnetic frustration is expected in the Ru1-Tb-Ru2 triangles, such as the red one.

Ru2 ions form independently uniform chains parallel to the b direction. The Ru-Ru length is 3.73 \AA in both the chains at 100 K. The Ru-O-Ru angles are 150.7° and 137.6° in the Ru1-Ru1 and Ru2-Ru2 pairs, respectively. When the Nd magnetic moments are ordered, the same internal magnetic fields are applied to the Ru sites in each chain. Regarding the change in the R sites due to the structural phase transition, the $R1$ and $R2$ sites in the low- T phase are the same in the high- T phase. The R_i ($i = 3 - 6$) sites in the low- T phase are the same in the high- T phase.

Next, we describe the magnetic properties of $R_3\text{RuO}_7$ ($R = \text{Tb}, \text{Gd}, \text{and Nd}$). We can observe a peak indicating an AF transition at $T_N = 17 \text{ K}$ and a broad maximum at

approximately 10 K in the specific heat of Tb_3RuO_7 [17]. The peak and maximum are speculated to indicate the ordering of the Ru and Tb moments, respectively. No hysteresis appears between the magnetizations measured in the zero-field cooling (ZFC) and field cooling (FC) processes in the magnetic field of $\mu_0 H = 0.1$ T. In the specific heat of Gd_3RuO_7 , two peaks exist at 15 and 9.5 K [18, 25]. It was speculated that the Ru and Gd moments were ordered below 15 and 9.5 K, respectively. We can see hysteresis between the magnetizations measured in the ZFC and FC processes at 0.05 and 0.1 T. In Nd_3RuO_7 , the specific heat exhibits a peak at 19 K [21]. Hysteresis exists between the magnetizations measured in the ZFC and FC processes at 0.1 T below 19 K. The magnetization curve at 5 K also shows hysteresis at $\mu_0 H < 2$ T. The hysteresis in the magnetization of Gd_3RuO_7 and Nd_3RuO_7 indicates the existence of small spontaneous magnetization (ferromagnetic component).

Powder neutron-diffraction measurements were performed on Nd_3RuO_7 [21], and the magnetic reflections were observed at 10 K. There are two types of propagation vectors $\mathbf{k}_1 = (0, 0, 0)$ and $\mathbf{k}_2 = (\frac{1}{2}, 0, 0)$ for the magnetic structure in the standard setting of the crystal structure. The a , b , and c axes in the published setting [21] correspond to the c , a , and b axes in the standard setting used in this study. Harada *et al.* considered that the magnetic reflections belonging to \mathbf{k}_1 were generated by the Ru ordered moments, and determined the magnetic structure of the Ru moments. The Ru moments are parallel to the a direction and are aligned antiferromagnetically in each chain. The magnitude of the Ru ordered moments was estimated to be $2.2 \mu_B$. The magnetic structure of the Nd moments has not been determined.

Different (nonuniform) internal magnetic fields are applied to the Ru1 and Ru2 sites when the Tb magnetic moments are ordered in Tb_3RuO_7 . An exotic magnetic structure is expected. The magnetic structure of Nd_3RuO_7 has not been determined but it is useful in understanding the magnetic structure of Tb_3RuO_7 . Consequently, we conducted powder neutron-diffraction experiments on Tb_3RuO_7 and Nd_3RuO_7 . The concentration of the magnetic ions is high in $R_3\text{RuO}_7$. If the magnetic entropy change is large, $R_3\text{RuO}_7$ behaves as a magnetic refrigeration material. Therefore, we investigated the magnetic entropy change in Tb_3RuO_7 and Gd_3RuO_7 , which have the large magnetic moments of rare-earth ions.

II. MATERIAL PREPARATION AND EXPERIMENTAL METHODS TO STUDY MAGNETISM

We synthesized the crystalline powders of $R_3\text{RuO}_7$ ($R = \text{Tb}, \text{Gd}, \text{and Nd}$) by using a solid-state reaction. The starting materials were $R_2\text{O}_3$ ($R = \text{Tb}, \text{Gd}, \text{and Nd}$), and RuO_2 powders. The purity was 99.99 %. A stoichiometric mixture of the powders was sintered in air. The sintering temperatures and time were 1473 K and 24 h for Tb_3RuO_7 and Gd_3RuO_7 , and 1523 K and 48 h for Nd_3RuO_7 , respectively. We measured the X-ray powder diffraction patterns at room temperature by using an X-ray diffractometer (RINT-TTR III, Rigaku). For Tb_3RuO_7 and Gd_3RuO_7 , the obtained samples were in single phases within experimental accuracy. For Nd_3RuO_7 , we observed some weak reflections, indicating the existence of other materials whose identities could not be determined.

We measured the magnetization using the magnetic property measurement system (MPMS) of Quantum Design. We carried out neutron-diffraction experiments at the Swiss Spallation Neutron Source of the Paul Scherrer Institut, where we used the high-resolution powder diffractometer for thermal neutrons [26]. The wavelength of the neutrons (λ) was 1.886 Å. We carried out group theory analyses of the magnetic structures using the programs ISODISTORT [27] and BasIreps in the FullProf Suite program package [28]. We performed Rietveld refinements of the crystal and magnetic structures using the FullProf Suite program package [28] containing internal tables for scattering lengths and magnetic form factors.

III. RESULTS

A. Magnetization

Figure 2 depicts the T dependence of the magnetization [$M(T)$] of Tb_3RuO_7 and Nd_3RuO_7 measured in a magnetic field of $\mu_0 H = 0.01$ T. Hysteresis appears between the magnetizations measured in the ZFC and FC processes at low temperatures. In Tb_3RuO_7 , no hysteresis was reported in the magnetization result measured at 0.1 T [17]. We were able to observe the hysteresis because of the small magnetic field (0.01 T). The hysteresis indicates the existence of a tiny spontaneous magnetization.

Figure 3 shows the magnetic entropy changes [$-\Delta S_m(T)$] of Tb_3RuO_7 and Gd_3RuO_7 for various strengths of the magnetic field. We measured $M(T)$ in the magnetic fields of 0.01

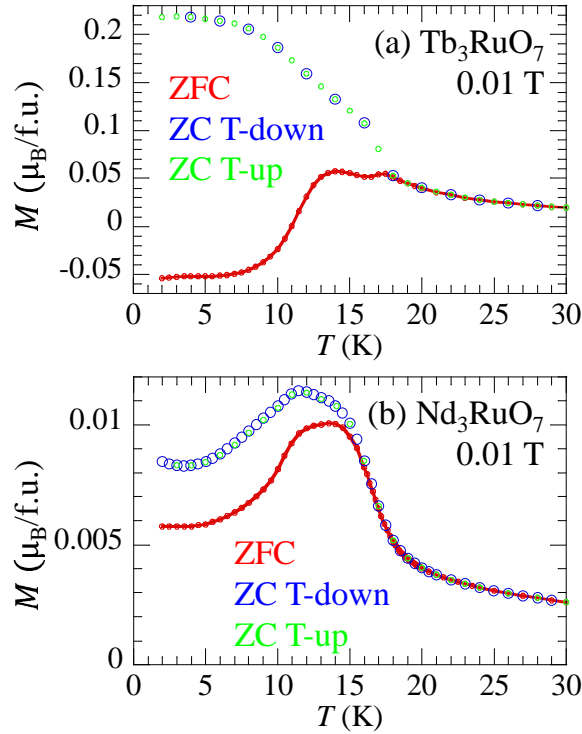


FIG. 2: Temperature dependence of the magnetization $[M(T)]$ of (a) Tb_3RuO_7 and (b) Nd_3RuO_7 in a magnetic field of $\mu_0 H = 0.01$ T. Red, blue, and green circles represent $M(T)$ measured in zero-field cooling (ZFC), field cooling (FC), and field warming processes, respectively.

T and 0.5 – 5 T in steps of 0.5 T. We derived $-\Delta S_m(T)$ from the Maxwell relation

$$-\Delta S_m(T) = \int_0^H \left(-\frac{\partial M(T)}{\partial T} \right)_H dH. \quad (1)$$

The red line in each figure indicates $-\Delta S_m(T)$ for the magnetic field change of 5 T. Broad maxima are apparent at approximately 19 K and 11 K for Tb_3RuO_7 and Gd_3RuO_7 , respectively.

B. Magnetic structure of Tb_3RuO_7

Figure 4 depicts the powder neutron-diffraction patterns of Tb_3RuO_7 at 1.5 and 25 K. Some reflections are observed only at 1.5 K and the other reflections are observed both at 1.5 and 25 K. The former reflections appear below 15 K. Therefore, these are magnetic reflections. Several magnetic reflections are larger or comparable to the largest nuclear

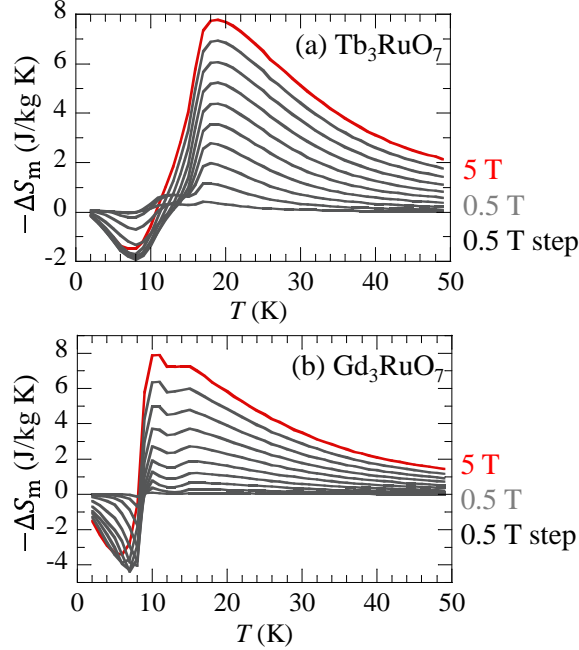


FIG. 3: Magnetic entropy change in (a) Tb₃RuO₇ and (b) Gd₃RuO₇ with change in magnetic field from 0.5 to 5 T in steps of 0.5 T.

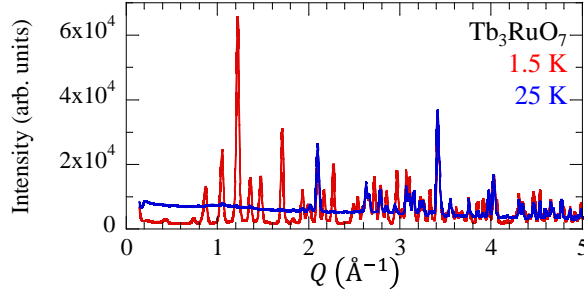


FIG. 4: Powder neutron-diffraction patterns of Tb₃RuO₇ at 1.5 K and 25 K.

reflection. We can index all the magnetic reflections with the propagation vector $\mathbf{k}_1 = (0, 0, 0)$. Table I shows the results of the group theory analysis for \mathbf{k}_1 . There are four one-dimensional irreducible representations (IRs) that appear three times each.

We determined the magnetic structure of Tb₃RuO₇ as follows. The magnitude of the Tb moment ($g_J J = 9 \mu_B$) is larger than that of the Ru moment ($gS \sim 3 \mu_B$). The magnetic reflections are generated mainly by the Tb ordered moments because the magnitude of the magnetic reflections is proportional to the square of the magnetic moments. Therefore, we

TABLE I: Group theory analysis for the magnetic structure of Tb_3RuO_7 calculated using the programs ISODISTORT [27] and BasIreps [28]. The character set corresponds to the following four symmetry elements [28]: Symm(1): 1; Symm(2): 2 (0, 0, 1/2) 0, 0, z ; Symm(3): a (1/2, 0, 0) x , 1/4, z ; Symm(4): n (0, 1/2, 1/2) 1/4, y , z . IR denotes irreducible representation. The crystallographic space group is $Pna2_1$ (No. 33). The magnetic propagation vector is $\mathbf{k}_1 = (0, 0, 0)$. All the ions are located at $4a$ sites. The components of the magnetic moments are expressed using u , v , and w .

| Character set | (1, 1, 1, 1) | (1, 1, -1, -1) | (1, -1, 1, -1) | (1, -1, -1, 1) |
|---|-------------------------|-------------------------|-------------------------|-------------------------|
| IR (ISODISTORT) | $m\Gamma_1$ | $m\Gamma_2$ | $m\Gamma_4$ | $m\Gamma_3$ |
| IR (BasIreps) | IRrep(1) | IRrep(2) | IRrep(3) | IRrep(4) |
| (x, y, z) | $[u, v, w]$ | $[u, v, w]$ | $[u, v, w]$ | $[u, v, w]$ |
| $(\bar{x}, \bar{y}, z + \frac{1}{2})$ | $[\bar{u}, \bar{v}, w]$ | $[\bar{u}, \bar{v}, w]$ | $[u, v, \bar{w}]$ | $[u, v, \bar{w}]$ |
| $(x + \frac{1}{2}, \bar{y} + \frac{1}{2}, z)$ | $[\bar{u}, v, \bar{w}]$ | $[u, \bar{v}, w]$ | $[\bar{u}, v, \bar{w}]$ | $[u, \bar{v}, w]$ |
| $(\bar{x} + \frac{1}{2}, y + \frac{1}{2}, z + \frac{1}{2})$ | $[u, \bar{v}, \bar{w}]$ | $[\bar{u}, v, w]$ | $[\bar{u}, v, w]$ | $[u, \bar{v}, \bar{w}]$ |

first considered only the Tb moments. There are eighteen components of the Tb moments because of the six crystallographic Tb sites. It is not realistic to independently refine the eighteen components. In the high- T phase, the Tb1 and Tb2 sites are equivalent, and the Tbi ($i = 3 - 6$) sites are equivalent. Therefore, we assumed the constraints that the magnitudes of each component of the Tb1 and Tb2 moments are identical ($-\text{Tb1}j- = -\text{Tb2}j-$) and that $-\text{Tb3}j- = -\text{Tb4}j- = -\text{Tb5}j- = -\text{Tb6}j-$, where $j = u, v$, and w . We carried out Rietveld refinements using only the Tb moments for the pattern at 1.5 K. We found that the best-fit candidate was $m\Gamma_3$ and that the Tb1 u , Tb1 w , and Tb3 v components were negligible.

Next, we performed the Rietveld refinements using the Ru moments as well as the Tb moments for the pattern at 1.5 K. We evaluated that the v and w components of the Ru moments were finite and that the u components were negligible. The u components are ferromagnetic in $m\Gamma_3$. Therefore, the evaluation is consistent with the tiny spontaneous magnetization seen in Fig. 2. Figure 5 shows the T dependence of the magnitude of the Ru1 and Ru2 moments. It seems unphysical that the magnitude of the Ru2 moment at 15 K is larger than that at 1.5 K.

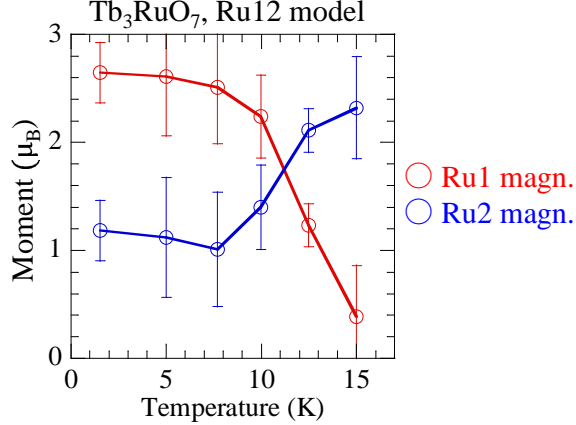


FIG. 5: Temperature dependence of the magnitudes of the Ru1 and Ru2 moments in Tb_3RuO_7 evaluated in Rietveld refinements using both the Ru1 and Ru2 moments (Ru12 model).

We considered other models with ordering of only the Ru1 moments (Ru1 model) and only the Ru2 moments (Ru2 model). The blue line in Fig. 6(a) indicates the result of Rietveld refinements using the Ru1 model, and can explain the observed diffraction pattern at 1.5 K (red circles). In contrast, the Ru2 model cannot explain the observed pattern well. The blue and green lines in Fig. 6(b) indicate the results of the Rietveld refinements using the Ru1 and Ru2 models, respectively. As is seen at around $Q = 0.43, 0.74$, and 0.96 \AA^{-1} , the consistency between the observed and refined patterns is better in the Ru1 model than in the Ru2 model.

Figure 7 shows the magnetic structure of Tb_3RuO_7 at 1.5 K. The Ru1 and Ru2 moments are ordered and disordered (paramagnetic), respectively, giving an appearance of a partially disordered (PD) state. The values of $|v|$ and $|w|$ of the Ru1 moments are $2.38(3)$ and $2.18(4) \mu_B$, respectively. The magnitude is $3.23(5) \mu_B$ and corresponds to $g = 2.15$. The order of the Tb1 and Tb2 moments is AF in each Tb1-Tb2 chain parallel to the b direction. The Tb1 and Tb2 ordered moments are parallel to the b direction and their magnitude is $8.58(2) \mu_B$. The Tb_i ($i = 3-6$) moments form a noncollinear magnetic structure. The values of $|u|$ and $|w|$ are $3.70(1)$ and $7.72(2) \mu_B$, respectively. The magnitude is $8.56(2) \mu_B$. The magnitude of all the Tb moments is slightly smaller than the theoretical value ($g_J J = 9 \mu_B$).

Figure 8 depicts the T dependence of the components and magnitudes of the ordered magnetic moments. Each component is almost constant below 10 K and decreases with in-

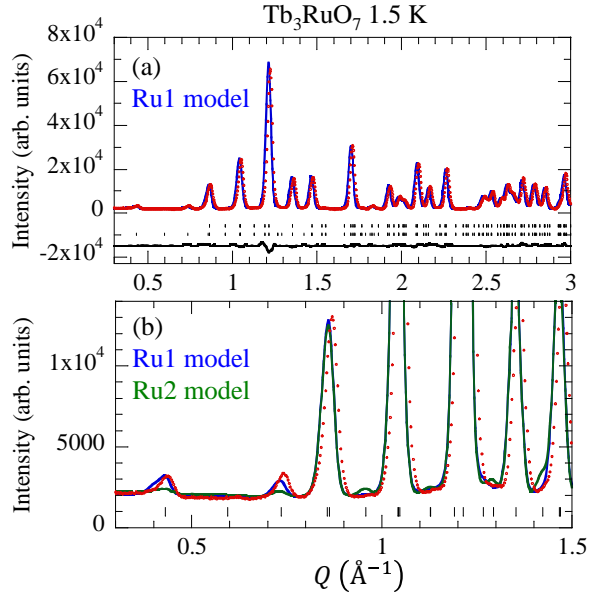


FIG. 6: Powder neutron-diffraction patterns (circles) at 1.5 K of Tb_3RuO_7 . (a) The line on the measured pattern portrays the Rietveld-refined pattern obtained using the Ru1 model. We used atomic parameters determined by Rietveld refinements for the pattern at 25 K using $Pna2_1$. The line at the bottom portrays the difference between the measured and Rietveld-refined patterns. The upper and lower hash marks represent the positions of the nuclear and magnetic reflections, respectively. The reliability indexes of the refinement are $R_p = 3.12\%$, $R_{wp} = 4.13\%$, and $R_{exp} = 0.77\%$. (b) The blue and green lines on the measured pattern portray the Rietveld-refined pattern obtained using the Ru1 and Ru2 models, respectively. The hash marks represent the positions of the magnetic reflections.

crease in T above 10 K. The v components decrease more rapidly than the other components. We speculated that the rotations of the Tb1 and Tb2 moments occurred at approximately 12.5 K. In contrast, the rotation of the Ru1 moment must be tiny because the v and w components are already considered and because the ferromagnetic u component must be negligible. We carried out Rietveld refinements on the diffraction pattern at 12.5 K by adding the Tb1 u , Tb1 w , Tb2 u , and Tb2 w components with the constraint that Tb1 u = -Tb2 u because of the tiny spontaneous magnetization. We evaluated that Tb1 u = -Tb2 u = 0.67(19), Tb1 w = 0.09(16), and Tb2 w = 0.45(17) in the unit of μ_B . The values of the other components were almost unchanged by adding these components. The magnitude of the

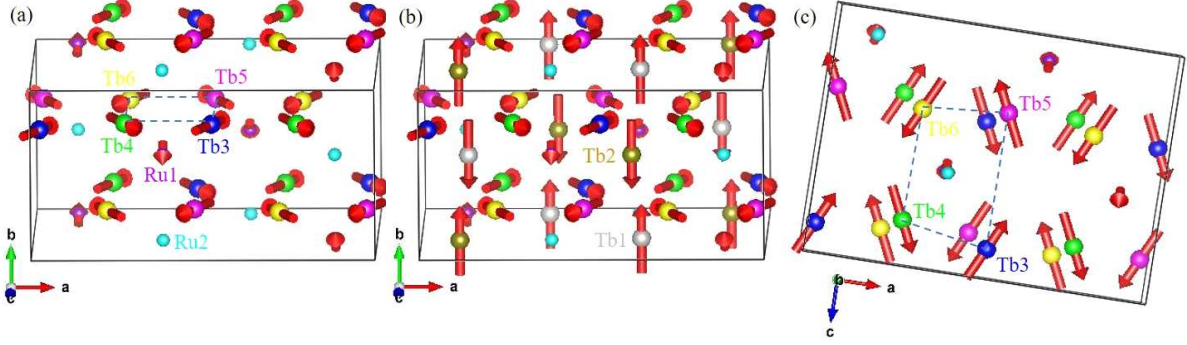


FIG. 7: Magnetic structure of Tb_3RuO_7 at 1.5 K, drawn using VESTA [24]. The IR is $m\Gamma_3$. The rectangle represents a unit cell. Tb1 and Tb2 are omitted in (a) and (c). The dashed lines in (a) and (c) represent a four-Tb ring, where the chiral vector is defined.

Tb1 v and Tb2 v components is $4.36(5)\mu_B$ and is much larger than that of the Tb1 u , Tb1 w , Tb2 u , and Tb2 w components. Therefore, any rotation of the Tb1 and Tb2 moments would be small. Next, we discuss the above specific-heat results [17]. The peak at $T_N = 17$ K and broad maximum at approximately 10 K in the specific heat were speculated to indicate the ordering of the Ru and Tb moments, respectively. We obtained the result that both the Ru1 and Tb moments were ordered at 15 K. No transition was observed between 15 K and 17 K. Therefore, both the Ru1 and Tb moments are ordered simultaneously at $T_N = 17$ K. The relatively rapid changes in the v components probably generated the broad maximum at approximately 10 K.

C. Magnetic structure of Nd_3RuO_7

Figure 9(a) depicts the powder neutron-diffraction patterns of Nd_3RuO_7 at 1.5 and 25 K. Some reflections are observed only at 1.5 K and the other reflections are observed both at 1.5 and 25 K. The former reflections appear below 17.5 K. Therefore, these are magnetic reflections. Our measurements confirmed the existence of two types of propagation vectors $\mathbf{k}_1 = (0, 0, 0)$ and $\mathbf{k}_2 = (\frac{1}{2}, 0, 0)$, as has been reported by Harada et al. [21]. The results of the group theory analysis calculated by the programs ISODISTORT [27] and BasIreps [28] are summarized in Table II. In comparison with Tb_3RuO_7 with only one magnetic propagation vector (\mathbf{k}_1) and all magnetic ions at the same crystallographic site ($4a$), the

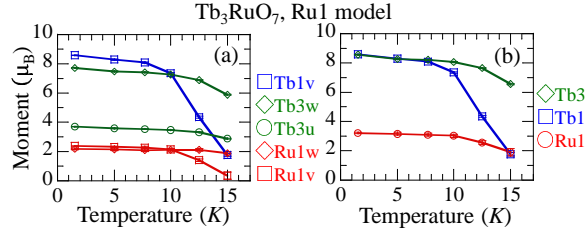


FIG. 8: (a) Temperature dependence of the components of the Ru1, Tb1, and Tb3 moments in Tb_3RuO_7 , evaluated in Rietveld refinements using the Ru1 model. In the Rietveld refinements, we used the constraints that $-\text{Tb1v}- = -\text{Tb2v}-$ and $-\text{Tbij}-$ ($i = 3 - 6$, $j = u$ and w) are identical. Although error bars are shown, they are not clearly visible in this scale of the moment. (b) Temperature dependence of the magnitudes of the Ru1, Tb1, and Tb3 moments.

situation in Nd_3RuO_7 is more complicated. There are two magnetic propagation vectors, and the magnetic ions are distributed across five different crystallographic sites.

We determined the magnetic structure of Nd_3RuO_7 as follows. As is seen in Fig. 9, there are several strong magnetic reflections for \mathbf{k}_1 , whereas all the magnetic reflections for \mathbf{k}_2 are weak. The difference indicates that most magnetic moments generate the magnetic reflections of \mathbf{k}_1 . After the initial Rietveld refinements, we found that the best-fit candidates for \mathbf{k}_1 and \mathbf{k}_2 were $m\Gamma_1^+$ and mY_1^+ , respectively, and that only the Ru1 moments obey mY_1^+ . Note that both $m\Gamma_1^+$ and mY_1^+ belong to the same character set, as shown in Table II.

It is not realistic to independently refine all the components of the magnetic moments. In the high- T phase, the Nd1 and Nd2 sites are equivalent, and the Ndi ($i = 3 - 6$) sites are equivalent. Therefore, we assumed the constraints that $-\text{Nd1j}- = -\text{Nd2j}-$ ($j = u, v$, and w) and $-\text{Nd}iv-$ ($i = 3 - 6$) are identical. $\text{Nd}iu$ and $\text{Nd}iw$ ($i = 3 - 6$) are zero because of symmetry. In $m\Gamma_1^+$, the v components are ferromagnetic and the source of the tiny spontaneous magnetization in $M(T)$. Thus, we assumed the additional constraints that $\text{Nd1v} = -\text{Nd2v}$, the sum of $\text{Nd}iv$ ($i = 3 - 6$) = 0, and $\text{Ru2v} = 0$. We conducted Rietveld refinements to determine the magnetic structure. The blue line in Fig. 9(b) indicates the results of the Rietveld refinements and can explain the observed diffraction pattern at 1.5 K (red circles).

Figure 10 shows the magnetic structure of Nd_3RuO_7 at 1.5 K. It is significantly different from the magnetic structure of Tb_3RuO_7 at 1.5 K despite the similar crystal structures. The

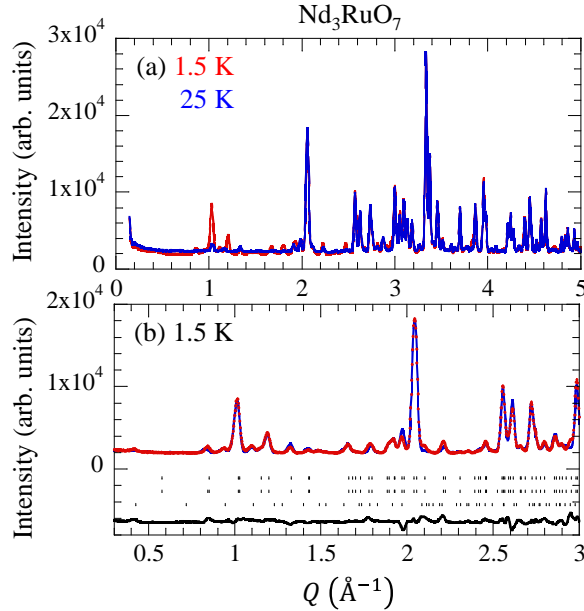


FIG. 9: (a) Powder neutron-diffraction patterns of Nd_3RuO_7 at 1.5 K and 25 K. (b) The results of Rietveld refinements for the pattern at 1.5 K (circles). We applied the atomic parameters determined by Rietveld refinements for the pattern at 25 K using $P2_1/m$. The line on the measured pattern portrays the Rietveld-refined pattern. The line at the bottom portrays the difference between the measured and Rietveld-refined patterns. The upper, middle, and lower hash marks represent the positions of nuclear reflections, magnetic reflections of \mathbf{k}_1 , and magnetic reflections of \mathbf{k}_2 . The reliability indexes of the refinement are $R_p = 5.01\%$, $R_{wp} = 6.70\%$, and $R_{exp} = 0.96\%$.

values of $|u|$ and $|w|$ of the Ru1 moments are 1.84(40) and 1.93(30) μ_B , respectively, and those of the Ru2 moments are 1.98(18) and 2.06(11) μ_B , respectively. The values of Ru1 v and Ru2 v are negligible. The magnitudes of the Ru1 and Ru2 moments are 2.67(50) and 2.86(21) μ_B , respectively, and is slightly smaller than the classical value ($\sim 3 \mu_B$), suggesting the existence of quantum fluctuation due to the one dimensionality. In contrast to Tb_3RuO_7 , no PD state of the Ru moments appears. The order of the Ru moments is AF in each chain parallel to the b direction. The AF alignment is consistent with the signs of the intrachain exchange interactions expected from the Ru-O-Ru angles (150.7° and 137.6°). The magnetic structures of the Ru1 and Ru2 moments indicate that the interchain exchange interactions along the a direction are antiferromagnetic and ferromagnetic, respectively. The present magnetic structure is different from the previously reported structure [21]. We performed

TABLE II: Group theory analysis for the magnetic structure of Nd_3RuO_7 calculated by the programs ISODISTORT [27] and BasIreps [28]. The character set corresponds to the following four symmetry elements [28]: Symm(1): 1; Symm(2): $2(0, 1/2, 0) 0, y, 0$; Symm(3): $\bar{1} 0, 0, 0$; Symm(4): $m x, 1/4, z$. IR denotes irreducible representation. The crystallographic space group is $P2_1/m$ (No. 11). The magnetic propagation vectors are $\mathbf{k}_1 = (0, 0, 0)$ and $\mathbf{k}_2 = (\frac{1}{2}, 0, 0)$. The components of the magnetic moments are expressed as u, v , and w . The blank cells indicate that the magnetic order of the moments on the corresponding site is impossible.

| Character set | (1, 1, 1, 1) | (1, 1, -1, -1) | (1, -1, 1, -1) | (1, -1, -1, 1) |
|---|---|---|-------------------------------------|-------------------------------------|
| Propagation vector | \mathbf{k}_1 \mathbf{k}_2 | \mathbf{k}_1 \mathbf{k}_2 | \mathbf{k}_1 \mathbf{k}_2 | \mathbf{k}_1 \mathbf{k}_2 |
| IR (ISODISTORT) | $m\Gamma_1^+$ mY_1^+ | $m\Gamma_1^-$ mY_1^- | $m\Gamma_2^+$ mY_2^+ | $m\Gamma_2^-$ mY_2^- |
| IR (BasIreps) | IRrep(1) | IRrep(2) | IRrep(3) | IRrep(4) |
| Ru1 $2c$ $(0, 0, \frac{1}{2})$ | $[u, v, w]$ $[u, v, w]$ | | $[u, v, w]$ $[u, v, w]$ | |
| $(0, \frac{1}{2}, \frac{1}{2})$ | $[\bar{u}, v, \bar{w}]$ $[\bar{u}, v, \bar{w}]$ | | $[u, \bar{v}, w]$ $[u, \bar{v}, w]$ | |
| Ru2 $2b$ $(\frac{1}{2}, 0, 0)$ | $[u, v, w]$ | $[u, v, w]$ | $[u, v, w]$ | $[u, v, w]$ |
| $(\frac{1}{2}, \frac{1}{2}, 0)$ | $[\bar{u}, v, \bar{w}]$ | $[u, \bar{v}, w]$ | $[u, \bar{v}, w]$ | $[\bar{u}, v, \bar{w}]$ |
| Nd1 $2d$ $(\frac{1}{2}, 0, \frac{1}{2})$ | $[u, v, w]$ | $[u, v, w]$ | $[u, v, w]$ | $[u, v, w]$ |
| $(\frac{1}{2}, \frac{1}{2}, \frac{1}{2})$ | $[\bar{u}, v, \bar{w}]$ | $[u, \bar{v}, w]$ | $[u, \bar{v}, w]$ | $[\bar{u}, v, \bar{w}]$ |
| Nd2 $2a$ $(0, 0, 0)$ | $[u, v, w]$ $[u, v, w]$ | | $[u, v, w]$ $[u, v, w]$ | |
| $(0, \frac{1}{2}, 0)$ | $[\bar{u}, v, \bar{w}]$ $[\bar{u}, v, \bar{w}]$ | | $[u, \bar{v}, w]$ $[u, \bar{v}, w]$ | |
| Nd3-Nd6 $2e$ $(x, \frac{1}{4}, z)$ | $[0, v, 0]$ $[0, v, 0]$ | $[u, 0, w]$ $[u, 0, w]$ | $[u, 0, w]$ $[u, 0, w]$ | $[0, v, 0]$ $[0, v, 0]$ |
| $(\bar{x}, \frac{3}{4}, \bar{z})$ | $[0, v, 0]$ $[0, v, 0]$ | $[\bar{u}, 0, \bar{w}]$ $[\bar{u}, 0, \bar{w}]$ | $[u, 0, w]$ $[u, 0, w]$ | $[0, \bar{v}, 0]$ $[0, \bar{v}, 0]$ |

Rietveld refinements for the magnetic reflections belonging to \mathbf{k}_1 by using moments other than the Ru1 moments, whereas Harada *et al.* performed Rietveld refinements using the Ru1 and Ru2 moments. Therefore, our results are different from those reported in their study.

The values of $|u|$ and $|w|$ of the Nd1 and Nd2 moments are 1.81(14) and 1.99(8) μ_B , respectively, whereas that of $|v|$ is negligible. The magnitude is 2.68(16) μ_B . The order of the Nd1 and Nd2 moments is AF in each chain parallel to the b direction. The magnitude of the $\text{Nd}i$ ($i = 3 - 6$) moments parallel to the b direction is 2.01(6) μ_B . The $\text{Nd}i$ ($i =$

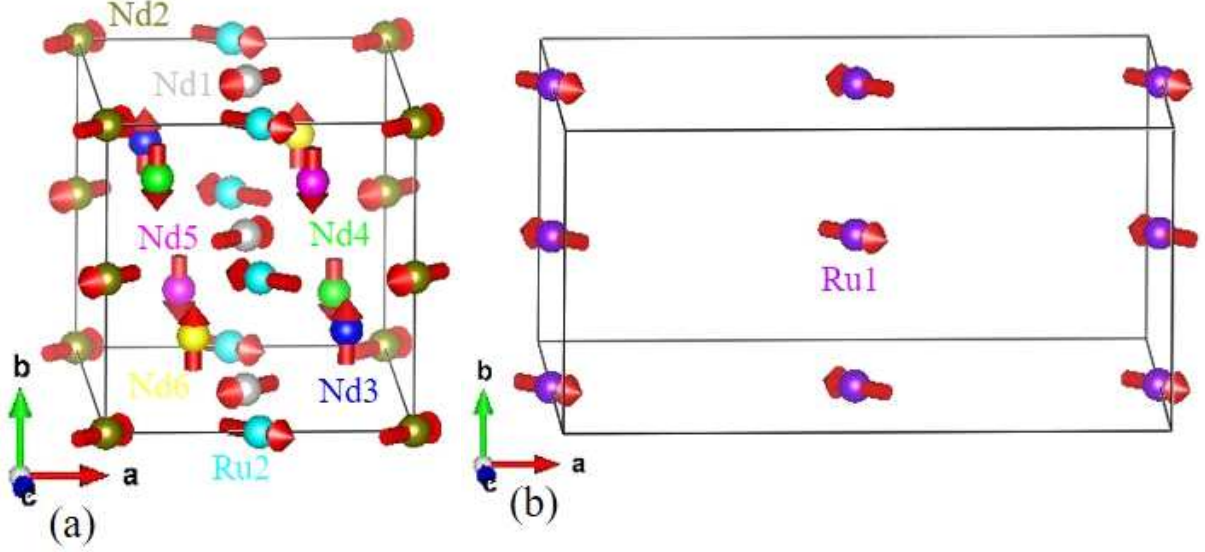


FIG. 10: Magnetic structure of Nd_3RuO_7 at 1.5 K, drawn using VESTA [24]. The IR is (a) $m\Gamma_1^+$ for $\mathbf{k}_1 = (0, 0, 0)$ and (b) mY_1^+ for $\mathbf{k}_2 = (\frac{1}{2}, 0, 0)$. The rectangle represents the magnetic unit cell.

3 – 6) moments form a collinear magnetic structure that is significantly different from the noncollinear magnetic structure of the Tbi ($i = 3-6$) moments in Tb_3RuO_7 . The theoretical value of the Nd moment ($g_J J = 3.27 \mu_B$) is slightly larger than those of the Nd1 and Nd2 moments, and is much larger than those of the Ndi ($i = 3-6$) moments.

Figure 11 depicts the T dependence of the components and magnitudes of the ordered magnetic moments. The magnitude of the Nd moments decrease to low values at 17.5 K, whereas that of the Ru moments remains large at 17.5 K. As T is lowered from $T_N = 19$ K, the Ru and Nd moments appear to increase rapidly and gradually, respectively.

IV. DISCUSSION

A. Magnetic entropy change

We compared the magnetic entropy changes of Tb_3RuO_7 and Gd_3RuO_7 with those of other oxides containing rare-earth ions. Figure 12 shows the maximum magnetic entropy change ($-\Delta S_{m,\text{max}}$) versus temperature (T_{max}) at which the magnetic entropy change is the maximum. The change in the magnetic field is 5 T. As a rough trend, $-\Delta S_{m,\text{max}}$ increases

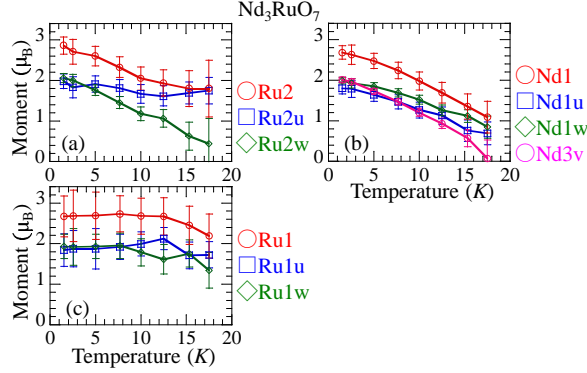


FIG. 11: Temperature dependence of the components and magnitude of magnetic moments in Nd_3RuO_7 , evaluated through Rietveld refinements; (a) Ru2, (b) Nd1 and Nd3, and (c) Ru1. In the Rietveld refinements, we used the constraints $-\text{Nd}1j- = -\text{Nd}2j-$, where $j = u$ and w , and $-\text{Nd}iv-$ ($i = 3 - 6$) are identical.

with decreasing T_{max} [41]. In Tb_3RuO_7 and Gd_3RuO_7 , the values of $-\Delta S_{\text{m,max}}$ are not very large for the values of T_{max} because the magnetic orders are not ferromagnetic in the two compounds.

B. Origin of the partially disordered state

We consider the origin of the PD state in Tb_3RuO_7 . As shown in Table III, several antiferromagnets possessing magnetic frustration in exchange interactions constitute the PD state. The materials belonging to group A have multiple crystallographic magnetic-ion sites. In the spin- $\frac{1}{2}$ frustrated three-leg-ladder Heisenberg antiferromagnets $\text{Cu}_3(\text{OH})_4\text{AO}_4$ ($A = \text{S}$ or Se), the Cu moments within the two outer legs are ordered, whereas the Cu moments within the inner leg remain random [42, 43]. In the spin- $\frac{1}{2}$ frustrated quasi-one-dimensional antiferromagnet $\text{Cu}_3\text{Mo}_2\text{O}_9$, the Cu moments within the dimers are ordered, whereas the Cu moments within the chains remain random [44]. The materials belonging to group C show a PD state in spite of a unique crystallographic magnetic-ion site.

Magnetic frustration in exchange interactions can exist in Tb_3RuO_7 . For example, let us consider the Ru1-Tb4-Ru2 triangle indicated in Fig. 1(c). There are eight similar Ru1-Tb-Ru2 triangles per Ru site. The Ru1-Ru2 interactions are probably AF based on the Ru1-O-Ru2 angles (141.6° and 145.5°). The interactions between the Ru and Tb moments

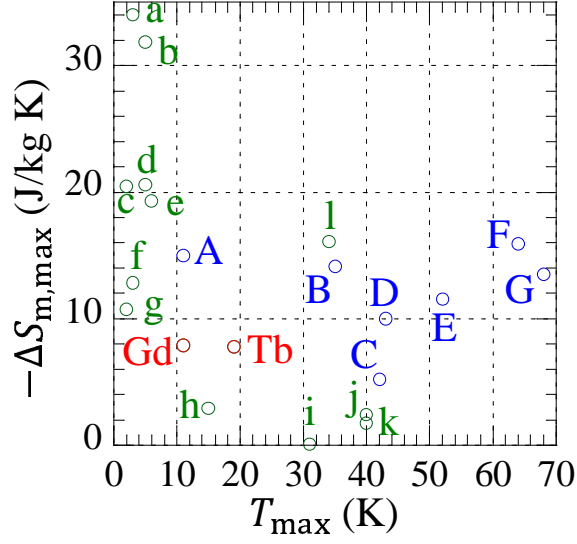


FIG. 12: $-\Delta S_{m,\max}$ versus T_{\max} of several oxides. Tb: Tb_3RuO_7 , Gd: Gd_3RuO_7 , a: GdFeO_3 [29], b: Ho_2O_3 [30], c: $\text{Er}_6\text{WO}_{12}$ [31], d: $\text{Ho}_6\text{WO}_{12}$ [31], e: $\text{Dy}_6\text{WO}_{12}$ [31], f: Gd_2O_3 [32], g: $\text{Sr}_2\text{DyNbO}_6$ [33], h: $\text{Tm}_6\text{MoO}_{12}$ [31], i: Sr_2YRuO_6 [33], j: $\text{Sr}_2\text{DyRuO}_6$ [33], k: $\text{Sr}_2\text{TbRuO}_6$ [33], l: $\text{Er}_2\text{Mn}_2\text{O}_7$ [34], A: TbMnO_3 ($H//a$) [35], B: GdTiO_3 ($H//c$) [36], C: YbTiO_3 ($H//c$) [37], D: ErTiO_3 ($H//c$) [37], E: HoTiO_3 ($H//c$) [38], F: DyTiO_3 ($H//c$) [39], G: TmTiO_3 ($H//c$) [40]. Lowercase and uppercase letters indicate the data for powders and single crystals, respectively.

TABLE III: Antiferromagnets showing a partially disordered (PD) state. The materials belonging to the groups A and B have multiple crystallographic magnetic-ion sites. The sites are clearly different from each other in group A, and are very similar to each other in group B. The materials belonging to group C have unique crystallographic magnetic-ion site.

| group A | group B | group C |
|--|---------------------------|---|
| $\text{Cu}_3(\text{OH})_4\text{SO}_4$ [42, 43] | Tb_3RuO_7 | CsCoCl_3 [45] |
| $\text{Cu}_3(\text{OH})_4\text{SeO}_4$ [43] | | CuFeO_2 [46] |
| $\text{Cu}_3\text{Mo}_2\text{O}_9$ [44] | | Ag_2CrO_2 [47] |
| | | $\text{Gd}_2\text{Ti}_2\text{O}_7$ [48] |
| | | GeNi_2O_4 [49] |

must exist because both the Ru1 and Tb moments are ordered at the same T (17 K). Magnetic frustration in the Ru1-Tb-Ru2 triangles is possible when the signs of the Ru1-Tb and Ru2-Tb interactions are the same. In contrast, it appears that the Ru-Ru interactions alone cannot generate magnetic frustration because of the following facts. The Ru1-Ru2 chains are almost linear and are well separated from one another. The next-nearest-neighbor Ru-Ru interaction in the chains and interchain interactions may be very weak.

We speculate that a chiral vector generated by four Tb moments may also be the origin of the magnetic frustration. The chiral vector is defined as

$$\mathbf{V}_c = \mathbf{M}_1 \times \mathbf{M}_2 + \mathbf{M}_2 \times \mathbf{M}_3 + \mathbf{M}_3 \times \mathbf{M}_4 + \mathbf{M}_4 \times \mathbf{M}_1, \quad (2)$$

where \mathbf{M}_i ($i = 1 - 4$) denote the magnetic moment vectors. For example, in the Tb4356 ring, indicated by the dashed lines in Fig. 7, we let the Tb4, Tb3, Tb5, and Tb6 moments correspond to \mathbf{M}_1 , \mathbf{M}_2 , \mathbf{M}_3 , and \mathbf{M}_4 , respectively. The chiral vector is calculated as $(0, 228, 0) \mu_B^2$ in the Tb4356 ring located at approximately $y \sim 0.75$. The directions of the Tb moment vectors in the Tb6534 ring located at approximately $y \sim 0.25$ are opposite to those of the respective Tb moment vectors in the Tb4356 ring connected by the dashed lines. The chiral vector is $(0, 228, 0) \mu_B^2$ in the Tb6534 ring as well. Consequently, the chiral vectors are parallel (ferromagnetic) along the b direction. The Ru1-Ru2 chains penetrate the rings formed by the four Tb sites. As described, AF exchange interactions are expected between the nearest-neighbor Ru1 and Ru2 spins in the chains. If the interaction between the chiral vector and Ru spin exists, magnetic frustration may occur. In contrast, in Nd_3RuO_7 , the $\text{Nd}i$ ($i = 3 - 6$) moments form a collinear magnetic structure. Therefore, no chiral vector exists.

We consider that the main source of the PD state in Tb_3RuO_7 is magnetic frustration in exchange interactions. However, all the Ru moments are ordered in Nd_3RuO_7 although a similar magnetic frustration can be expected. Considering materials with a unique crystallographic magnetic-ion site (group C), the absence of a PD state in Nd_3RuO_7 cannot be explained by the fact that the Ru sites in each chain are equivalent. The magnitude of the Nd moment ($g_J J = 3.27 \mu_B$) is smaller than that of the Tb moment ($9 \mu_B$). Therefore, the magnetic frustration may be weaker in Nd_3RuO_7 than in Tb_3RuO_7 , leading to the absence of a PD state in Nd_3RuO_7 . There is another difference between the two compounds. The internal magnetic field generated by the R ordered moments at the Ru1 sites is different

from that at the Ru2 sites in Tb_3RuO_7 , whereas the magnetic field is the same at the Ru sites in each chain of Nd_3RuO_7 . We speculate that the different (nonuniform) magnetic field increases the difference in the properties between the Ru1 and Ru2 moments (ordered and disordered, respectively).

V. SUMMARY

We performed powder neutron-diffraction experiments on Tb_3RuO_7 and Nd_3RuO_7 to determine the magnetic structures. There are two crystallographic Ru sites and six crystallographic R ($R = \text{Tb}$ or Nd) sites in the low- T phase. In Tb_3RuO_7 , alternating-bond spin- $\frac{3}{2}$ Ru1-Ru2 chains are formed parallel to the b direction. The Ru and Ru2 moments are ordered and disordered (paramagnetic), respectively, below 15 K. This result indicates the appearance of a PD state, although the two Ru sites are very similar to each other. The order of the Tb moments is AF in each Tb1-Tb2 chain parallel to the b direction. The $\text{Tb}i$ ($i = 3 - 6$) moments form a noncollinear magnetic structure. In Nd_3RuO_7 , the Ru1 and Ru2 ions form independently uniform chains parallel to the b direction. The order of the Ru moments is AF in each chain. The order of the Nd1 and Nd2 moments is also AF in each chain parallel to the b direction. The $\text{Nd}i$ ($i = 3 - 6$) moments form a collinear magnetic structure. The main cause of the PD state in Tb_3RuO_7 is probably the magnetic frustration in the exchange interactions. Based on the difference in the magnetic structures between Tb_3RuO_7 and Nd_3RuO_7 , we speculate that the chiral vector formed by the Tb3, Tb4, Tb5, and Tb6 moments may also generate magnetic frustration. The internal magnetic field generated by the Tb ordered moments at the Ru1 sites is different from that at the Ru2 sites. We speculate that the different (nonuniform) internal magnetic field increases the difference in the properties between the Ru1 and Ru2 moments.

We investigated the temperature dependence of the magnetic entropy changes of Tb_3RuO_7 and Gd_3RuO_7 . When the magnetic-field change is 5 T, broad maxima are observed at approximately $T_{\text{max}} = 19$ K and 11 K, and the maximum magnetic entropy changes ($-\Delta S_{\text{m,max}}$) are 7.78 and 7.92 J/(kg K) for Tb_3RuO_7 and Gd_3RuO_7 , respectively. The values of $-\Delta S_{\text{m,max}}$ are not very large for the values of T_{max} because the magnetic orders are not ferromagnetic in the two compounds.

Acknowledgments

This work was supported by the Japan Society for the Promotion of Science (JSPS) KAKENHI Grant Number 18K03551, a grant for advanced measurement and characterization technologies accelerating materials innovation (PF2050) from National Institute for Materials Science (NIMS), and JST-Mirai Program Grant Number JPMJMI18A3, Japan. We are grateful to Takashi Mochiku, Hiroaki Mamiya, Masamichi Nishino, Noriki Terada, and Naohito Tsujii at NIMS for the fruitful discussions, and to Seiko Matsumoto at NIMS for the sample syntheses and X-ray diffraction measurements. We would like to thank Editage (www.editage.com) for English language editing.

-
- [1] D. C. Dender, P. R. Hammar, D. H. Reich, C. Broholm, and G. Aeppli, Direct Observation of Field-Induced Incommensurate Fluctuations in a One-Dimensional $S = \frac{1}{2}$ Antiferromagnet, *Phys. Rev. Lett.* **79**, 1750 (1997).
- [2] K. Nagata, Short range order effects on EPR frequencies in antiferromagnets with inequivalent g -tensors, *J. Phys. Soc. Jpn.* **40**, 1209 (1976).
- [3] T. Asano, H. Nojiri, Y. Inagaki, J. P. Boucher, T. Sakon, Y. Ajiro, and M. Motokawa, ESR Investigation on the Breather Mode and the Spinon-Breather Dynamical Crossover in Cu Benzoate, *Phys. Rev. Lett.* **84**, 5880 (2000).
- [4] H. Nojiri, Y. Ajiro, T. Asano, and J. P. Boucher, Magnetic excitation of $S = \frac{1}{2}$ antiferromagnetic spin chain Cu benzoate in high magnetic fields, *New J. Phys.* **8**, 218 (2006).
- [5] M. Kenzelmann, Y. Chen, C. Broholm, D. H. Reich, and Y. Qiu, Bound Spinons in an Antiferromagnetic $S = \frac{1}{2}$ Chain with a Staggered Field, *Phys. Rev. Lett.* **93**, 017204 (2004).
- [6] M. Kenzelmann, C. D. Batista, Y. Chen, C. Broholm, D. H. Reich, S. Park, and Y. Qiu, $S = \frac{1}{2}$ chain in a staggered field: High-energy bound-spinon state and the effects of a discrete lattice, *Phys. Rev. B* **71**, 094411 (2005).
- [7] M. Oshikawa, K. Ueda, H. Aoki, A. Ochiai, and M. Kohgi, Field-Induced Gap Formation in Yb_4As_3 , *J. Phys. Soc. Jpn.* **68**, 3181 (1999).
- [8] M. Kohgi, K. Iwasa, J. M. Mignot, B. Fåk, P. Gegenwart, M. Lang, A. Ochiai, H. Aoki, and T. Suzuki, Staggered Field Effect on the One-Dimensional $S = \frac{1}{2}$ Antiferromagnet Yb_4As_3 , *Phys. Rev. Lett.* **86**, 2439 (2001).
- [9] R. Feyerherm, S. Abens, D. Günther, T. Ishida, M. Meißner, M. Meschke, T. Nogami, and M. Steiner, Magnetic-field induced gap and staggered susceptibility in the $S = \frac{1}{2}$ chain $[\text{PM} \cdot \text{Cu}(\text{NO}_3)_2 \cdot (\text{H}_2\text{O})_2]_n$ (PM = pyrimidine), *J. Phys.: Condens.Matter* **12**, 8495 (2000).
- [10] S. A. Zvyagin, A. K. Kolezhuk, J. Krzystek, and R. Feyerherm, Excitation Hierarchy of the Quantum Sine-Gordon Spin Chain in a Strong Magnetic Field, *Phys. Rev. Lett* **93**, 027201 (2004).
- [11] A. U. B. Wolter, H. Rakoto, M. Costes, A. Honecker, W. Brenig, A. Klümper, H.-H. Klauss, F. J. Litterst, R. Feyerherm, D. Jérôme, and S. Süllow, High-field magnetization study of the $S = \frac{1}{2}$ antiferromagnetic Heisenberg chain $[\text{PM} \text{ Cu}(\text{NO}_3)_2(\text{H}_2\text{O})_2]_n$ with a field-induced gap,

- Phys. Rev. B **68**, 220406(R) (2003).
- [12] A. U. B. Wolter, P. Wzietek, S. Süllow, F. J. Litterst, A. Honecker, W. Brenig, R. Fey-
erherm, and H.-H. Klauss, Giant Spin Canting in the $S = \frac{1}{2}$ Antiferromagnetic Chain
[CuPM(NO₃)₂(H₂O)₂]_n Observed by ¹³C-NMR, Phys. Rev. Lett. **94**, 057204 (2005).
- [13] R. Morisaki, T. Ono, H. Tanaka, and H. Nojiri, Thermodynamic properties and elementary
excitations in quantum sine-Gordon spin system KCuGaF₆, J. Phys. Soc. Jpn. **76**, 063706
(2007).
- [14] I. Umegaki, H. Tanaka, T. Ono, H. Uekusa, and H. Nojiri, Elementary excitations of the
 $S = \frac{1}{2}$ one-dimensional antiferromagnet KCuGaF₆ in a magnetic field and quantum sine-
Gordon model, Phys. Rev. B **79**, 184401 (2009).
- [15] I. Umegaki, H. Tanaka, T. Ono, M. Oshikawa, and K. Sakai, Thermodynamic properties of
quantum sine-Gordon spin chain system KCuGaF₆, Phys. Rev. B **85**, 144423 (2012).
- [16] I. Umegaki, H. Tanaka, N. Kurita, T. Ono, M. Laver, C. Niedermayer, C. Rüegg, S. Ohira-
Kawamura, K. Nakajima, and K. Kakurai, Spinon, soliton, and breather in the spin- $\frac{1}{2}$ anti-
ferromagnetic chain compound KCuGaF₆, Phys. Rev. B **92**, 174412 (2015).
- [17] Y. Hinatsu and Y. Doi, Structural phase transition and antiferromagnetic transition of
Tb₃RuO₇, J. Solid State Chem. **220**, 22 (2014).
- [18] R. P. Bontchev, A. J. Jacobson, M. M. Gospodinov, V. Skumryev, V. N. Popov, B. Lorenz, R.
L. Meng, A. P. Litvinchuk, and M. N. Iliev, Crystal structure, electric and magnetic properties,
and Raman spectroscopy of Gd₃RuO₇, Phys. Rev. B **62**, 12235 (2000).
- [19] N. Ishizawa, K. Tateishi, S. Kondo, and T. Suwa, Structural phase transition of Gd₃RuO₇,
Inorg. Chem. **47**, 558 (2008).
- [20] W. A. Groen, F. P. F. van Berkel, and D. J. W. IJdo, Trineodymium ruthenate(V). A Rietveld
refinement of neutron powder diffraction data, Acta Crystallogr. C **43**, 2262 (1987).
- [21] D. Harada, Y. Hinatsu, and Y. Ishii, Studies on the magnetic and structural phase transitions
of Nd₃RuO₇, J. Phys.: Condens. Matter **13**, 10825(2001).
- [22] M. Wakeshima and Y. Hinatsu, Magnetic properties and structural transitions of orthorhombic
fluorite-related compounds Ln₃MO₇ (Ln = rare earths, M = transition metals), J. Solid State
Chem. **183**, 2681 (2010).
- [23] T. Ida, K. Hiraga, H. Hibino, S. Oishi, D. du Boulay, and N. Ishizawa, A non-centrosymmetric
polymorph of Gd₃RuO₇, Acta Crystallogr. E **62**, i13 (2006).

- [24] K. Momma and F. Izumi, VESTA for three-dimensional visualization of crystal, volumetric and morphology data, *J. Appl. Cryst.* **44**, 1272 (2011).
- [25] D. Harada and Y. Hinatsu, Magnetic and calorimetric studies on one-dimensional Ln_3RuO_7 ($Ln = Pr, Gd$), *J Solid State Chem.* **164**, 163 (2002).
- [26] P. Fischer, G. Frey, M. Koch, M. Koennecke, V. Pomjakushin, J. Schefer, R. Thut, N. Schlumpf, R. Buerge, U. Greuter, S. Bondt, and E. Berruyer, High-resolution powder diffractometer HRPT for thermal neutrons at SINQ, *Physica B* **276-278**, 146 (2000); [<http://sinq.web.psi.ch/hrpt>].
- [27] B. J. Campbell, H. T. Stokes, D. E. Tanner, and D. M. Hatch, ISODISPLACE: An internet tool for exploring structural distortions, *J. Appl. Cryst.* **39**, 607 (2006); [<https://stokes.byu.edu/iso/isodistort.php>].
- [28] J. Rodriguez-Carvajal, Recent advances in magnetic structure determination by neutron powder diffraction, *Physica B* **192**, 55 (1993); [<http://www.ill.eu/sites/fullprof/>].
- [29] M. Das, S. Roy, and P. Mandal, Giant reversible magnetocaloric effect in a multiferroic $GdFeO_3$ single crystal, *Phys. Rev. B* **96**, 174405 (2017).
- [30] A. Boutahar, R. Mouba, E. K. Hlil, H. Lassri, E. Lorenzo, Large reversible magnetocaloric effect in antiferromagnetic Ho_2O_3 powders, *Sci. Rep.* **7**, 13904 (2017).
- [31] M. Hase, N. Tsujii, H. S. Suzuki, O. Sakai, and H. Mamiya, Magnetic properties of oxides with high concentrations of rare-earth elements R_6AO_{12} ($R =$ rare-earth element, $A = Mo$ or W), *J. Magn. Magn. Mater.* **523**, 167539 (2021).
- [32] R. Paul, T. Paramanik, K. Das, P. Sen, B. Satpati, I. Das, Magnetocaloric effect at cryogenic temperature in gadolinium oxide nanotubes, *J. Magn. Magn. Mater.* **417**, 182 (2016).
- [33] M. Hase, N. Tsujii, and H. Mamiya, Magnetocaloric effect in the double perovskites Sr_2RRuO_6 ($R = Dy$ and Tb), *J. Jpn. Soc. Powder powder metallurgy* **67**, 182 (2020)
- [34] Y. Q. Cai, Y. Y. Jiao, Q. Cui, J. W. Cai, Y. Li, B. S. Wang, M. T. Fernández-Díaz, M. A. McCuire, J.-Q. Yan, J. A. Alonso, J.-G. Cheng, Giant reversible magnetocaloric effect in the pyrochlore $Er_2Mn_2O_7$ due to a cooperative two-sublattice ferromagnetic order, *Phys. Rev. Mater.* **1**, 064408 (2017).
- [35] J.-L. Jin, X.-Q. Zhang, G.-K. Li, Z.-H. Cheng, L. Zheng, and Y. Lu, Giant anisotropy of magnetocaloric effect in $TbMnO_3$ single crystals, *Phys. Rev. B* **83**, 184431 (2011).
- [36] H. Omote, S. Watanabe, K. Matsumoto, I. Gilmutdinov, A. Kiiamov, D. Tayurskii, Magne-

- totaloric effect in single crystal GdTiO₃, *Cryogenics* **101**, 58 (2019).
- [37] Y. Su, Y. Sui, J.-G. Cheng, J.-S. Zhou, X. Wang, Y. Wang, and J. B. Goodenough, Critical behavior of ferromagnetic perovskites RTiO₃ (R = Dy, Ho, Er, Tm, Yb) by magnetocaloric measurements, *Phys. Rev. B* **87**, 195102 (2013).
- [38] Y. Su, Y. Sui, J. Cheng, X. Wang, Y. Wang, W. Liu, and X. Liu, Large reversible magnetocaloric effect in HoTiO₃ single crystal, *J. Appl. Phys.* **110**, 083912 (2011).
- [39] Y. Su, Y. Sui, X. Wang, J. Cheng, Y. Wang, W. Liu, and X. Liu, Large magnetocaloric properties in single-crystal dysprosium titanate, *Mater. Lett.* **72**, 15 (2012).
- [40] Y. Su, Y. Sui, J. Cheng, X. Wang, Y. Wang, P. Liu, and J. Tang, Large reversible magnetocaloric effect in TmTiO₃ single crystal, *J. Appl. Phys.* **111**, 07A925 (2012).
- [41] As a review article, V. Franco, J. S. Blázquez, J. J. Ipus, J. Y. Law, L. M. Moreno-Ramírez, and A. Conde, Magnetocaloric effect: From materials research to refrigeration devices, *Progr. Mater. Sci.* **93**, 112 (2018).
- [42] S. Vilminot, M. Richard-Plouet, G. André, D. Swierczynski, M. Guillot, F. Bourée-Vigneron, and M. Drillon, Magnetic structure and properties of Cu₃(OH)₄SO₄ made of triple chains of spins $s = \frac{1}{2}$, *J. Solid State Chem.* **170**, 255 (2003).
- [43] S. Vilminot, G. André, F. Bourée-Vigneron, M. Richard-Plouet, and M. Kurmoo, Magnetic properties and magnetic structures of Cu₃(OH)₄XO₄, X = Se or S: Cycloidal versus collinear antiferromagnetic structure, *Inorg. Chem.* **46**, 10079 (2007).
- [44] M. Hase, H. Kuroe, V. Yu. Pomjakushin, L. Keller, R. Tamura, and N. Terada Y. Matsushita, A. Dönni, and T. Sekine, Magnetic structure of the spin- $\frac{1}{2}$ frustrated quasi-one-dimensional antiferromagnet Cu₃Mo₂O₉: Appearance of a partially disordered state, *Phys. Rev B* **92**, 054425 (2015).
- [45] M. Mekata, Antiferro-ferrimagnetic transition in triangular Ising lattice, *J. Phys. Soc. Jpn.* **42**, 76 (1977).
- [46] M. Mekata, N. Yaguchi, T. Takagi, T. Sugino, S. Mitsuda, H. Yoshizawa, N. Hosoito, and T. Shinjo, Successive magnetic ordering in CuFeO₂ -A new type of partially disordered phase in a triangular lattice antiferromagnet, *J. Phys. Soc. Jpn.* **62**, 4474 (1993).
- [47] M. Matsuda, C. de la Cruz, H. Yoshida, M. Isobe, R. S. Fishman, Partially disordered state and spin-lattice coupling in an $S = \frac{3}{2}$ triangular lattice antiferromagnet Ag₂CrO₂, *Phys. Rev B* **85**, 144407 (2012).

- [48] J. R. Stewart, G. Ehlers, A. S. Wills, S. T. Bramwell, and J. S. Gardner, Phase transitions, partial disorder and multi- k structures in $\text{Gd}_2\text{Ti}_2\text{O}_7$, *J. Phys.: Condens. Matter* **16**, L321 (2004).
- [49] M. Matsuda, J.-H. Chung, S. Park, T. J. Sato, K. Matsuno, H. Aruga Katori, H. Takagi, K. Kakurai, K. Kamazawa, Y. Tsunoda, I. Kagomiya, C. L. Henley, and S.-H. Lee, Frustrated minority spins in GeNi_2O_4 , *Europhys. Lett.* **82**, 37006 (2008).